 CMES, vol.75, no.2, pp.113-139, 2011

The Importance of Adequate Turbulence Modeling in Fluid Flows

L.Q. Moreira[1], F.P. Mariano[2] and A. Silveira-Neto[1]

Abstract: Turbulence in fluid flow is one of the most challenging problems in classical physics. It is a very important research problem because of its numerous implications, such as industrial applications that involve processes using mixtures of components, heat transfer and lubrication and injection of fuel into the combustion chambers and propulsion systems of airplanes. Turbulence in flow presents characteristics that are fully nonlinear and that occur at high Reynolds numbers. Because of the nonlinear nature of turbulent flow, an increase in the Reynolds number implies an increase in the Kolmogorov wave numbers, and the flow spectrum becomes larger in both length and time scales. Because of the variety of frequencies and wave numbers involved in turbulent flows, the computational cost becomes prohibitive. An alternative is to solve part of the frequency spectrum; the other part must be modeled. In this context, the Navier-Stokes equations must be filtered, modeled and solved based on the large eddy simulation (*LES*) methodology. The part of the spectrum related to the higher frequencies or wave numbers that is not solved must be modeled. In the present work, the [Smagorinsky (1963)] model and the dynamic Smagorinsky model [Germano, Piomelli, and Moin (1991)] were used. The goal is to show the importance of turbulence modeling in the simulation of turbulent flows. The problem of homogeneous isotropic turbulence in a periodic box was chosen. There are several ways to model and simulate this flow, and in the present work, a body force was added to the Navier-Stokes equations in order to model the injection of energy at low wave numbers. Because of the energy cascade, the energy injected to the large structures is transferred to the small structures to achieve the Kolmogorov dissipative scales. When the energy spectrum reaches steady state, it is maintained at equilibrium. Many values were used for the Smagorinsky model constant (C_s), yielding an excessive energy transfer for

[1] Universidade Federal de Uberlândia - UFU, Faculdade de Engenharia Mecânica - FEMEC, Av.: João Naves de Ávila, 2121, Campus Santa Mônica, Bl.:5P, CEP: 38400-902, Uberlândia, MG, Brasil, lqmoreira@mecanica.ufu.br; aristeus@mecanica.ufu.br

[2] Escola de Engenharia Elétrica e Computação, Universidade Federal de Goiás, Av.: Universitária, 1488, Qd.: 86, Bl.: A, Setor Leste Universitário, Goiânia, GO, Brasil

$C_s = 0.30$ and an insufficient energy transfer for $C_s = 0.10$. Therefore, energy was accumulated at the higher wave number of the spectrum. The value $C_s = 0.18$ was determined to be acceptable. This value is the same one that was determined analytically by [Lilly (1992)]. The mean value $C_s = 0.12$ was determined using the dynamic Smagorinsky model simulation.

Keywords: Computational Fluid Dynamics, Fourier Pseudo-Spectral Method, Large Eddy Simulation, Isotropic Turbulence.

1 Introduction

Turbulence in fluid flows has been a challenging subject of research for several decades and remains one of the most difficult problems. Understanding the associated phenomena is of great importance because of the large number of natural and industrial applications. These applications range from the flows inside a bubble or a drop [Ceniceros, Roma, Silveira-Neto, and Villar (2010); Villar (2007)], pair of cylinders [Silva, Silveira-Neto, Francis, Rade, and Santos (2009)] to the flows over vehicles or aircraft [Vedovoto (2007)] submarines, fuel mixtures inside a turbine, geophysical flows and even the motion of galaxies [Maier, Iapichino, Schmidt, and Niemeyer (2009); Parrish, Quataert, and Sharma (2010)]. One way to study turbulence is through computational fluid dynamics (*CFD*), in which a set of numerical methods are used solve the Navier-Stokes equations [White (1991)]. These equations are capable of modeling flows and representing the associated physical phenomena. *CFD* was first developed in the 60-th. Because of the evolution of numerical methods and the increase in processing power, the *CFD* tool allows one to study complex phenomena that require great computational power, which is the case for turbulent flows. The numerical solution of the Navier-Stokes equations can be accomplished using several methods: the finite difference, the finite volume, the finite element, Lattice boltzmann method [Chen, Chang, and Sun (2007)] and the spectral methods [Mariano, Moreira, da Silveira-Neto, da Silva, and Pereira (2010)].

Depending on the flow that one wishes to solve or the physical phenomenon that one wishes to study, one of these methods will be more suitable than others. The search for accurate methods is of great interest to fluid dynamics researchers because there are physical phenomena for which only high-precision methods yield a satisfactory solution to the problem; for instance, phenomena like aero-acoustics, combustion and transition to turbulence. The main difficulty in obtaining the solution of the Navier-Stokes equations with high accuracy is the computational cost involved. In the case of turbulent flows, which constitute the great majority of flows, it may be impracticable or even impossible to obtain a solution. To circumvent this

problem, we solve a part of the spectrum, the low frequencies structures of the flow, and model the part related to physical phenomena characterized by frequencies and wave numbers larger than the cutoff frequency or cutoff wave number.

The present paper aims to demonstrate the need for and the importance of adequately modeling the effects of turbulence. For this, homogeneous and isotropic turbulence flows that develop in a periodic cubic box will be studied. The Smagorinsky and dynamic Smagorinsky models were used and compared with the Kolmogorov law. For the Smagorinsky model, the importance of adjusting the constant (C_s) is studied in order to avoid energy accumulation in the sub-grid scales or avoid excessive energy transfer. The search for the correct value of this constant is a computationally onerous job and depends on the type of flow and on the numerical code used. Several studies comment on the values of this constant [Canuto and Cheng (1997); Lesieur, Métais, and Comte (2005); da Silva and Pereira (2005)]. Another problem is that this constant depends on the numerical scheme and on the computational code used. Finally, an alternative way to calculate the Smagorinsky constant is presented.

2 Mathematical Modeling

2.1 The filtered Navier-Stokes equations for turbulence

The mass and momentum balance equations for the incompressible flow of a Newtonian fluid are given by:

$$\frac{\partial u_i}{\partial x_i} = 0, \tag{1}$$

$$\frac{\partial u_i}{\partial t} = -\frac{\partial}{\partial x_j}(u_i u_j) - \frac{1}{\rho}\frac{\partial p}{\partial x_i} + \frac{\partial}{\partial x_j}\left[\nu\left(\frac{\partial u_i}{\partial x_j} + \frac{\partial u_j}{\partial x_i}\right)\right] + \frac{f_i}{\rho}, \tag{2}$$

where x_i is the i-th component of the position vector $\boldsymbol{x}$, u_i is the i-th component of the velocity vector $\boldsymbol{u}$, $\nu = \mu/\rho$ is the kinematic viscosity, μ is the dynamic viscosity, ρ is the specific mass, f_i is the i-th component of the vector force $\boldsymbol{f}$ and p is the pressure. The numerical solution of Eqs. 1 and 2, taking into account all the scales that compose a given turbulent flow, is possible, and is characterized by the approach called direct numerical simulation (*DNS*). However, because of the high number of degrees of freedom in turbulent flow, this type of resolution almost always requires prohibitive computational costs and is only feasible for flows at moderate Reynolds numbers values.

The numerical solution of 1 and 2 becomes feasible for high Reynolds numbers by the decomposition of the flow variables into two bands of scales through a filtering process that separates the solved scales $\left(\overline{\phi}(\boldsymbol{x},t)\right)$ from the sub-grid scales

$(\phi'(\boldsymbol{x},t))$. This decomposition, based on the principle of the large eddy simulation (*LES*) methodology, is given by Eq. 3:

$$\phi(\boldsymbol{x},t) = \overline{\phi}(\boldsymbol{x},t) + \phi'(\boldsymbol{x},t), \tag{3}$$

where $\phi(\boldsymbol{x},t)$ is the function to be decomposed, $\overline{\phi}(\boldsymbol{x},t)$ is the filtered or the largest scale and $\phi'(\boldsymbol{x},t)$ is the smallest scale or sub-grid structure of turbulence. The filtered part is defined as the convolution integral of the function to be filtered, $\phi(\boldsymbol{x},t)$, by a filter function, $G(\boldsymbol{x},t)$, i.e.:

$$\overline{\phi}(\boldsymbol{x},t) = \int \phi(\boldsymbol{x},t)\, G(\boldsymbol{x}-\boldsymbol{x}')d\boldsymbol{x}', \tag{4}$$

where the filter function $(G(\boldsymbol{x},t))$ as used in the present work is a cutoff function, given by:

$$G(|\boldsymbol{x}|) = \begin{cases} 1/\forall & \text{if} \quad |\boldsymbol{x}| \leq x_c \\ \\ 0 & \text{if} \quad |\boldsymbol{x}| > x_c \end{cases}. \tag{5}$$

The vector $\boldsymbol{x}$ represents the position of a fluid article, x_c is the cutoff length of the filter, $\forall$ is the volume over which the filtering process is performed and $G(\boldsymbol{x})$ is the filter function in physical space. Applying the filtering process to Eqs. 1 and 2, they take the following forms, as specified in [Lesieur (1997)]:

$$\frac{\partial \bar{u}_i}{\partial x_i} = 0, \tag{6}$$

$$\frac{\partial \bar{u}_i}{\partial t} + \frac{\partial}{\partial x_j}(\bar{u}_i \bar{u}_j) = -\frac{1}{\rho}\frac{\partial \bar{p}}{\partial x_i} + \frac{\partial}{\partial x_j}\left[\nu\left(\frac{\partial \bar{u}_i}{\partial x_j} + \frac{\partial \bar{u}_j}{\partial x_i}\right) - \tau_{ij}\right] + \frac{\bar{f}_i}{\rho}. \tag{7}$$

The influence of the resolved scales on the sub-grid scales appear in the global sub-grid tensor (τ_{ij}), defined as:

$$\tau_{ij} \equiv \overline{u_i u_j} - \bar{u}_i \bar{u}_j. \tag{8}$$

This sub-grid tensor is to be modeled. In the present paper, it is modeled using the classical method proposed by Boussinesq, $\left(\tau_{ij} - \frac{1}{3}\kappa \bar{S}_{ij} = -2\nu_t \bar{S}_{ij}\right)$, where κ is the kinetic energy of turbulence, ν_t is the kinematic turbulent viscosity and $\left(\bar{S}_{ij} = \frac{1}{2}\left(\frac{\partial \bar{u}_i}{\partial x_j} + \frac{\partial \bar{u}_j}{\partial x_i}\right)\right)$ is the filtered strain rate tensor. The absence or incorrect modeling of the tensor τ_{ij} implies improper energy transfer between the solved turbulent structures and the sub-grid scales or scales smaller than the cutoff wave

number. Applying the definition of the global sub-grid tensor in Eq. 8 and using the model proposed by Boussinesq, Eq. 9 is obtained as follows:

$$\frac{\partial \bar{u}_i}{\partial t} + \frac{\partial}{\partial x_j}(\bar{u}_i \bar{u}_j) = -\frac{1}{\rho}\frac{\partial \bar{p}*}{\partial x_i} + \frac{\partial}{\partial x_j}\left[(\nu + \nu_t)\left(\frac{\partial \bar{u}_i}{\partial x_j} + \frac{\partial \bar{u}_j}{\partial x_i}\right)\right] + \frac{\bar{f}_i}{\rho}, \tag{9}$$

where $\left(\bar{p}* = \bar{p} + \frac{2}{3}\rho\kappa\right)$ is the effective pressure and κ is the sub-grid scale kinetic energy. In the present work, the [Smagorinsky (1963)] model and the dynamic Smagorinsky model by [Germano, Piomelli, and Moin (1991)] will be used to calculate the turbulent viscosity, which is necessary to close the system of equations (Eqs. 6 and 9). The [Smagorinsky (1963)] model is based on the hypothesis of local equilibrium for small scales. The turbulent stress production is equal to the viscous dissipation. The production rate of stress can be written as a function of the shear rate calculated with the filtered velocity field, and the dissipation is a function of the velocity and the sub-grid length scales. Therefore, the turbulent viscosity proposed by Smagorinsky is given by:

$$\nu_t = (C_s\Delta)^2\sqrt{2\bar{S}_{ij}\bar{S}_{ij}}, \tag{10}$$

where C_s is the Smagorinsky constant and Δ is the characteristic length given by:

$$\Delta = \sqrt[3]{\prod_{l=1}^{3}\Delta x_l}. \tag{11}$$

The Smagorinsky constant (C_s) should be adjusted because it depends on the numerical method and on the type of flow. This task is computationally onerous; however, in the literature, there is a consensus about some of the values of this constant: for example, $C_s = 0.18$ for homogeneous isotropic turbulence [Lesieur, Métais, and Comte (2005); da Silva and Pereira (2005)], and $C_s = 0.13$ for free shear flows [da Silva and Pereira (2005)]. Depending on the application, C_s can vary in the range $0.05 \leq C_s \leq 0.30$. The adjustment of the Smagorinsky constant does not address the negative effects in parietal flow, such as excessive turbulent viscosity. The remedy for this problem is to use a damping function near the walls in order to have zero turbulent viscosity in this region of the flow.

The main drawbacks of the Smagorinsky model is that it uses direct cascading and does not allow the inverse cascading of turbulent kinetic energy. Moreover, in complex flows, such as in rotating flows or in regions near the boundary layer separation, the hypothesis of global equilibrium is not true. Another deficiency is that the model is not applicable for simulating turbulence transition. However, the Smagorinsky model represents the turbulent kinetic energy spectrum and the energy

cascade in free shear flows very well, given that the Smagorinsky constant is quite well adjusted. The dynamic Smagorinsky model [Germano, Piomelli, and Moin (1991)] is an enhanced version of the model proposed by [Smagorinsky (1963)], where the proportionality constant (C_s) is replaced by the proportionality function C_{sd}, which is dynamically calculated at each time point and at each position of the domain. This function must be calculated from the solution obtained for the velocity field, which is subjected to a test filter. The test filter, symbolically represented by $(\urcorner)$, must have a size cutoff greater than the grid filter cutoff size given by Eq. 11. Thus, all the variables required for the calculation of the proportionality function are available as follows [Lilly (1992)]:

$$\nu_t = C_{sd}(\boldsymbol{x},t)\Delta^2\sqrt{2\bar{S}_{ij}\bar{S}_{ij}}, \tag{12}$$

$$C_{sd}(\boldsymbol{x},t) = -\frac{1}{2}\frac{M_{ij}L_{ij}}{M_{ij}M_{ij}}, \tag{13}$$

$$L_{ij} = \overline{\bar{u}_i\bar{u}_j} - \overline{\bar{u}_i}\,\overline{\bar{u}_j}, \tag{14}$$

$$M_{ij} = \overline{\bar{\Delta}^2\left\|\bar{S}\right\|}\,\overline{\bar{S}_{ij}} - \overline{\bar{\Delta}^2\left\|\bar{S}\right\|\bar{S}_{ij}}, \tag{15}$$

where $\left\|\bar{S}\right\| = \sqrt{2\bar{S}_{ij}\bar{S}_{ij}}$ is the norm of the strain rate tensor. The calculation of C_{sd}, performed dynamically, makes it possible to obtain even negative values locally. This means that the model allows for an inverse cascade of energy. Moreover, a negative viscosity is a source of instability of the numerical schemes. To circumvent this problem, one assumes that the sum of the turbulent viscosity and the molecular viscosity is greater than or equal to zero. This assumption does not imply a guaranteed fidelity of the model but only partially allows for the inverse energy transfer. In modeling anisotropic flows at walls, the proportionality function makes the sub-grid tensor equal to zero automatically. Indeed, the tensor L_{ij} only depends on the velocities, which are zero at the walls. This is a great advantage, avoiding the need for additional damping models.

2.2 The filtered Navier-Stokes equation in Fourier space

To proceed with the transformation of Eqs. 6 and 9 to Fourier space and the return to physical space, the direct and inverse Fourier transform is used. This transform can be applied to any function in three dimensions and is given by:

$$\widehat{\phi}(\boldsymbol{k},t) = \int_{-\infty}^{\infty} \phi(\boldsymbol{x},t)\, e^{-\imath 2\pi \boldsymbol{k}\cdot\boldsymbol{x}} d\boldsymbol{x}, \tag{16}$$

$$\phi(\boldsymbol{x},t) = \int_{-\infty}^{\infty} \widehat{\phi}(\boldsymbol{k},t)\, e^{\imath 2\pi \boldsymbol{k}\cdot\boldsymbol{x}} d\boldsymbol{k}. \tag{17}$$

In these equations, $\widehat{\phi}(\boldsymbol{k},t)$ is the transformed function in Fourier space, $\phi(\boldsymbol{x},t)$ is the function in physical space, $\boldsymbol{k}$ is the wave number vector, which is the parameter for transformation to the Fourier space, and $\imath = \sqrt{-1}$ is the imaginary number. Applying the direct Fourier transform to Eqs. 6 and 9, the following equations result:

$$\imath k_i \widehat{\bar{u}}_i = 0 \tag{18}$$

$$\begin{aligned}\frac{\partial \widehat{\bar{u}}_i(\boldsymbol{k},t)}{\partial t} &= -\frac{1}{\rho}\imath k_i \widehat{\bar{p}} - \imath k_j \int_{\boldsymbol{k}=\boldsymbol{r}+\boldsymbol{s}} \widehat{\bar{u}}_i(\boldsymbol{r})\, \widehat{\bar{u}}_j(\boldsymbol{k}-\boldsymbol{r})\, d\boldsymbol{r} \\ &\quad -\imath k_j \int_{\boldsymbol{k}=\boldsymbol{r}+\boldsymbol{s}} \widehat{\nu_{ef}}(\boldsymbol{r}) \left[(k_j - r_j)\, \widehat{\bar{u}}_i + (k_i - r_i)\, \widehat{\bar{u}}_j\right](\boldsymbol{k}-\boldsymbol{r})\, d\boldsymbol{r} + \frac{\widehat{\bar{f}}_i}{\rho}\end{aligned} \tag{19}$$

where $\boldsymbol{k}$, $\boldsymbol{r}$ and $\boldsymbol{s}$ are the wave number vectors, the parameters of the Fourier transform. It is worth stressing that in the present work, the viscous term is considered in its complete form. Figure 1 illustrates the geometric representation of the terms of Eq. 19 with respect to the plane of zero divergence, called plane π, , which is defined in such a way that the wave number vector $\boldsymbol{k}$ is perpendicular to it. This definition is a consequence of Eq. 18, which shows that a velocity field in Fourier space for incompressible flows is orthogonal to the wave number vector and therefore belongs to the plane π. As the left side of Eq. 19 belongs to the plane π, except the pressure term, which is perpendicular to the plane π. Thus, the Eq. 19 can be rewritten as follows:

$$\begin{aligned}\frac{\partial \widehat{\bar{u}}_i(\boldsymbol{k},t)}{\partial t} &= \wp_{im}\Bigg\{-\imath k_j \int_{\boldsymbol{k}=\boldsymbol{r}+\boldsymbol{s}} \widehat{\bar{u}_m}(\boldsymbol{r})\, \widehat{\bar{u}}_j(\boldsymbol{k}-\boldsymbol{r})\, d\boldsymbol{r} \\ &\quad -\imath k_j \int_{\boldsymbol{k}=\boldsymbol{r}+\boldsymbol{s}} \widehat{\nu_{ef}}(\boldsymbol{r})\,(k_j - r_j)\widehat{\bar{u}_m}(\boldsymbol{k}-\boldsymbol{r})\, d\boldsymbol{r} \\ &\quad -\imath k_j \int_{\boldsymbol{k}=\boldsymbol{r}+\boldsymbol{s}} \widehat{\nu_{ef}}(\boldsymbol{r})\,(k_m - r_m)\widehat{\bar{u}}_j(\boldsymbol{k}-\boldsymbol{r})\, d\boldsymbol{r} + \frac{\widehat{f_m}}{\rho}\Bigg\},\end{aligned} \tag{20}$$

where

$$\wp_{im} = \delta_{im} - \frac{k_i k_m}{k^2} \tag{21}$$

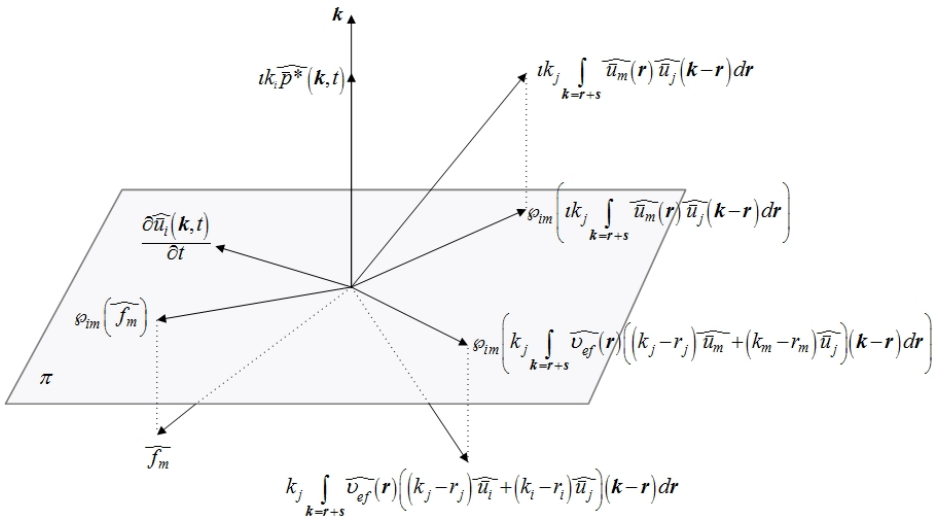

Figure 1: Representation of the terms of Eq. 19 in Fourier space and its representation relative to the plane π.

is the projection tensor operator, which projects any vector onto the plane π where δ_{im} is the Kronecker delta tensor.

Thus, the filtered global equations for the turbulence in Fourier space (Eq. 20) do not depend on the pressure field, unlike what happens in physical space. Therefore, the projection method minimizes the cost of the calculations for solving the Navier-Stokes equations for incompressible flows once it is not necessary to work with the pressure-velocity coupling. The need for solving the linear systems, the part that normally requires the greatest computational effort in conventional methodologies, is then not necessary. However, the pressure field can be obtained by mathematical manipulation of Eq. 19; and the procedure can be found in [Moreira (2007)]. The convolution integrals that appear in the nonlinear transformation terms are computationally expensive to calculate. As an alternative way to solve this problem, the pseudo spectral method is presented.

2.3 The Fourier pseudo-spectral method

The main idea of the Fourier pseudo-spectral method (*FPSM*) involves not directly computing the nonlinear advective and diffusive terms of Eq. 20 in Fourier space that would imply the resolution of the convolution integrals. The solution of a convolution integral is very expensive computationally. To solve this problem, all the spatial derivatives of the advective and diffusive (nonlinear) terms are calculated

in the Fourier space and are transformed to the physical space where all products are calculated. To illustrate the pseudo-spectral method, we take two functions $\boldsymbol{f}(\boldsymbol{x},t)$ and $\boldsymbol{g}(\boldsymbol{x},t)$. The Fourier transform of the product of these two functions is given by the following convolution integral:

$$\widehat{\boldsymbol{fg}}(\boldsymbol{k},t) = \int\limits_{\boldsymbol{k}=\boldsymbol{r}+\boldsymbol{s}} \widehat{\boldsymbol{f}}(\boldsymbol{r})\widehat{\boldsymbol{g}}(\boldsymbol{k}-\boldsymbol{r})d\boldsymbol{r}. \tag{22}$$

Another way to calculate this product is to compute the product of $\boldsymbol{f}$ by $\boldsymbol{g}$ in the physical space, creating a new function $\boldsymbol{h}(\boldsymbol{x},t) = \boldsymbol{f}(\boldsymbol{x},t)\boldsymbol{g}(\boldsymbol{x},t)$, which is then transformed to Fourier space:

$$\widehat{\boldsymbol{h}}(\boldsymbol{k},t) = \int\limits_{-\infty}^{\infty} \boldsymbol{h}(\boldsymbol{x},t)\, e^{-\imath 2\pi \boldsymbol{k}\cdot\boldsymbol{x}} d\boldsymbol{x}. \tag{23}$$

Calculating the Fourier transform of $\boldsymbol{h}(\boldsymbol{x},t)$, Eq. 23, is equivalent to performing the convolution integral of Eq. 22. Consequently, the Fourier transform of the derivative of the product is given by:

$$\frac{\partial(\boldsymbol{fg})}{\partial x_i} = \imath k_i \widehat{\boldsymbol{fg}} = \imath k_i \widehat{\boldsymbol{h}}. \tag{24}$$

In the case of the nonlinear advective and nonlinear viscous terms, we also have the presence of derivatives. In order to transform these terms, we use Eq. 24. For instance, if $\widehat{\boldsymbol{f}}(\boldsymbol{k},t)$ and $\widehat{\boldsymbol{g}}(\boldsymbol{k},t)$ are known in Fourier space, we perform the inverse transform to physical space, obtaining $\boldsymbol{f}(\boldsymbol{x},t)$ and $\boldsymbol{g}(\boldsymbol{x},t)$. Then, we calculate the product $\boldsymbol{f}(\boldsymbol{x},t)$ by $\boldsymbol{g}(\boldsymbol{x},t)$, yielding $\boldsymbol{h}(\boldsymbol{x},t)$, transform it to the Fourier space and then obtain $\widehat{\boldsymbol{h}}(\boldsymbol{k},t)$. Finally, we obtain the derivative $\imath\boldsymbol{k}\widehat{\boldsymbol{h}}(\boldsymbol{k},t)$ without calculating the convolution integral but also without loss of the accuracy of the spectral derivative calculation.

2.4 Numerical Method

In this section, the main numerical details used in the present work will be provided. The dimension of the physical domain in the x direction is L_x, which can be discretised using N_x collocation points equally spaced at a distance of $\Delta x = L_x/N_x$. Therefore, the position of a point is given by $x = n\Delta x$, where $1 \leq n \leq N_x$. In the spectral domain, we define a wave number vector the component x of which is $k_x = \frac{2\pi}{\lambda_x}$ where λ_x is the wave length. The step of the wave number in the spectral domain is given by $\Delta k_x = \frac{2\pi}{L_x}$, and thus, for the cutoff wave number, (k_c), the bigger resolved wave number is $max[k_x] = \frac{\pi N_x}{L_x} = \frac{\pi}{\Delta x}$ and the smaller is $min[k_x] = \frac{2\pi}{L_x}$. The

smallest resolved structure has a size of $2\Delta x$, and the largest has a size L_x. The same procedure applies to the directions y and z. A discrete Fourier transform (*DFT*) is the proper numerical way to evaluate Eq. 16. The *DFT* of a function ϕ is defined by Briggs and Henson (1995) as:

$$\widehat{\phi}_k = \sum_{n=\frac{-N}{2}+1}^{\frac{N}{2}} \phi_n e^{\frac{-\imath 2\pi kn}{N}}, \tag{25}$$

and Eq. 17 is evaluated using the discrete inverse Fourier transform (*DIFT*):

$$\phi_n = \frac{1}{N} \sum_{k=\frac{-N}{2}+1}^{\frac{N}{2}} \widehat{\phi}_k e^{\frac{\imath 2\pi kn}{N}}, \tag{26}$$

where $-N/2+1 \leq k \leq N/2$, k is the wave number vector and N is the number of collocation points in the discretised domain.

The application of a *DFT* is restricted to periodic boundary condition problems, limiting the use of the numerical Fourier transform in *CFD* to a restraint class of physical problems. Therefore, the Fourier spectral method has only been used for simulations of temporal jets, temporal mixing layers and homogeneous and isotropic turbulence, where:

$$\phi(\boldsymbol{x},t) = \phi(\boldsymbol{x}+\boldsymbol{L},t). \tag{27}$$

The fast Fourier transform (*FFT*) algorithm, applied to solve Eqs. 25 and 26, is very efficient and was proposed by [Cooley and Tukey (1965)]. In terms of floating point operations, when the *DFT* is performed using the *FFT* algorithm, it has a computational cost of $O(Nlog_2^N)$, which is very competitive with other computational methods that are $O(N^2)$.In the present paper, we used the $FFTE$ subroutine, which was implemented by [Takahashi (2006)]. The same procedure can be performed in order to perform the fast inverse Fourier transform. For the time evolution, the low-dissipation and low-dispersion fourth-order Runge-Kutta algorithm proposed by [Allampalli, Hixon, Nallasamy, and Sawyer (2009)] was chosen in order to maintain the accuracy.

3 Results

3.1 Verification of the computational code

The synthesisation method of analytical solutions for a differential model is an interesting concept, which enables one to obtain a solution as a safe reference in

order to verify methodologies and algorithms. The synthesis consists of adding a source term to a differential equation to propose a plausible analytical solution and, through applying the analytical solution in the differential model, determining the source term. Therefore, we have a differential model with a known analytical solution [Silva, Souza, and Medeiros (2007)].

The following analytical periodic solution for the Navier-Stokes equations, with constant physical properties, including a source term, was proposed by [Henshaw (1994)]:

$$u^a(x,y,z,t) = \sin(x)\cos(y)\cos(z)\cos(2\pi t) \tag{28}$$

$$v^a(x,y,z,t) = \cos(x)\sin(y)\cos(z)\cos(2\pi t) \tag{29}$$

$$w^a(x,y,z,t) = -2\cos(x)\cos(y)\sin(z)\cos(2\pi t) \tag{30}$$

$$p^a(x,y,z,t) = \sin(x)\sin(y)\sin(z)\cos(2\pi t)\,. \tag{31}$$

The source terms to be added to the momentum equations are obtained by solving the derivatives that appear in Eq. 32:

$$f_i = \frac{\partial u_i^a}{\partial t} + \frac{\partial}{\partial x_j}\left(u_i^a u_j^a\right) + \frac{1}{\rho}\frac{\partial p^a}{\partial x_i} + \frac{\partial}{\partial x_j}\left[\nu\left(\frac{\partial u_i^a}{\partial x_j} + \frac{\partial u_j^a}{\partial x_i}\right)\right], \tag{32}$$

where the super-index a stands for the analytical solution, given by Eqs. 28-31. The fields u^a, v^a and w^a satisfy Eq. 1. Introducing these solutions into Eq. 32, the field $\boldsymbol{f}(\boldsymbol{x},t)$ can be obtained. Thus, for a problem given by Eqs. 1 and 2, with a known source term $\boldsymbol{f}(\boldsymbol{x},t)$, the analytical solution is given by Eqs. 28-31. To evaluate the results quantitatively, the norm L_2 is used, which measures the error between the variable numerically calculated (ϕ^c) and the variables analytically calculated (ϕ^a) as follows:

$$L_2 = \sqrt{\frac{1}{N_x N_y N_z}\sum_{i=1}^{N_x}\sum_{j=1}^{N_y}\sum_{k=1}^{N_z}\left[\phi^c(x_i,y_j,z_k,t) - \phi^a(x_i,y_j,z_k,t)\right]^2}. \tag{33}$$

Note that although the norm has been defined with respect to a generic function ϕ, it can be used for all velocity components and for the pressure field, replacing by the variable of interest in Eq. 33. The super-index c stands for the fields numerically calculated.

The reference parameters that model the problem are the vortex diameter, $L_r = \pi[m]$, the maximum velocity of the flow that occurs at time $t = 0[s]$, $U_r = max[u^a(\boldsymbol{x})$,

$v^a(\boldsymbol{x}), w^a(\boldsymbol{x})] = 1.0[m/s]$ and the reference time that is given by $t_r = L_r/U_r = \pi[s]$. The Reynolds number for this flow is given by Eq. 34:

$$Re = \frac{U_r L_r}{\nu}, \tag{34}$$

which makes it possible to calculate the viscosity ν of the fluid. As the goal of this simulation is to verify the algorithm, its implementation and to show the accuracy of *FPSM*, the differences between the calculated and analytical velocity fields were quantified using the L_2 norm defined in Eq. 33. All the simulations presented in this section were performed in a calculation domain of $L_x = L_y = L_z = 2\pi$ and $Re = 10$. In the first simulation, a constant time step of $\Delta t = 10^{-4}[s]$ was used, the simulated time was set at $10[s]$ and 8^3, 16^3 and 32^3 collocation nodes were used. As shown in Fig. 2, the error is of round-off (10^{-15}) level, and there are no significant differences in the results for the different grids. This level of error characterizes a methodology with spectral accuracy and spectral rate of convergence. Thus, for the other simulations, a mesh of 32^3 collocation nodes was used.

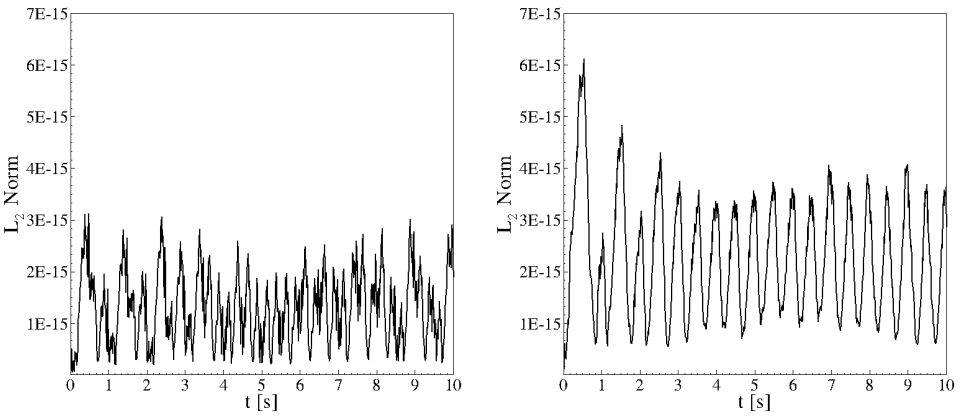

(a) (b)

Figure 2: Influence of the collocation point number on the temporal evolution of the norm L_2 of the w component of the velocity with (a) 8^3 or (b) 32^3 collocation points.

To study the influence of the size of the time step, three cases with $\Delta t = 10^{-3}[s]$, $10^{-4}[s]$ and $10^{-5}[s]$ were simulated. Note that the errors found with $\Delta t = 10^{-4}[s]$ and $10^{-5}[s]$ are of the order 10^{-15}, which is close to the machine round-off error. Note that the error for $\Delta t = 10^{-3}[s]$ is larger compared with the other time steps. The goal of these results was to demonstrate that the time steps used do not introduce large errors into the spatial solution. The results of Fig. 3 show that the error

for $10^{-4}[s]$ and $10^{-5[s]}$ is of the order of the machine round-off error. Thus, the time step $\Delta t = 10^{-4}[s]$ will be used hereafter.

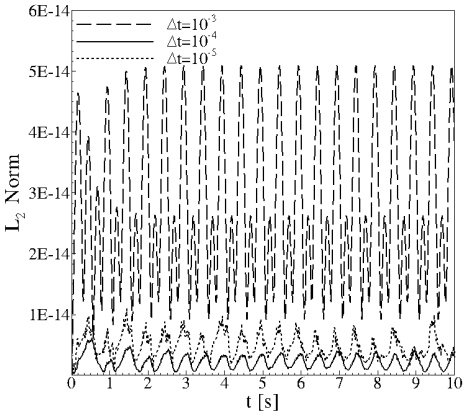

Figure 3: Influence of the time step in the temporal evolution of the norm L_2 of the w component of velocity.

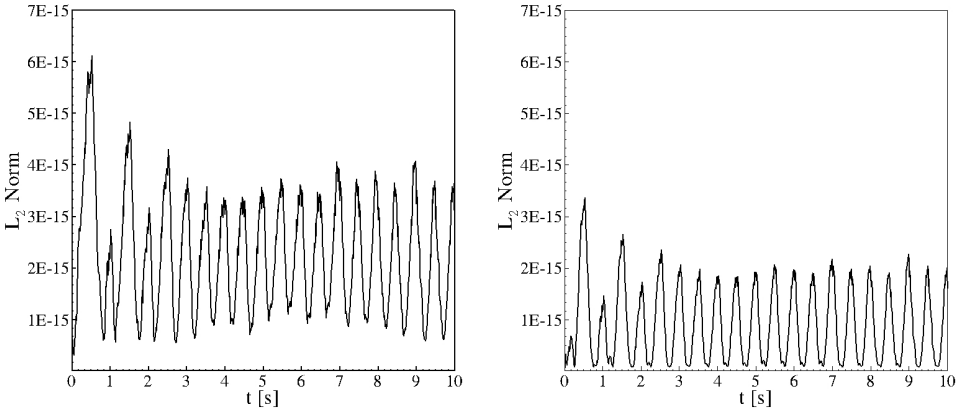

(a) (b)

Figure 4: Temporal evolution of the L_2 norm for the following: (a) component z of the velocity and (b) the pressure.

Figure 4 shows the temporal evolution of the norm L_2 for the z component of velocity and pressure. Note that for both velocity component in Fig. 4 (a) and the pressure in Fig. 4 (b), the L_2 norm is of the order 10^{-15}, which corresponds to the machine round-off error using double precision. The velocity components in the x

and y directions also presented errors on the order of the machine round-off error, demonstrating the high precision of *FPSM*. In solving the Navier-Stokes equations for incompressible flows with the numerical method used, it is very difficult to keep the same order of errors and convergence for both pressure and velocity. Another very important result is that the pressure presents the same order of convergence as the velocity components.

3.2 Isotropic Turbulence

Once the numerical code against a synthesized analytical solution is verified, the validation of the developed numerical code against benchmark results was performed. The physical laws must be obeyed, as pointed out by [(Silva, Souza, and Medeiros, 2007)].

The authors of the present work have a particular interest in studies of turbulent flows. One of the most common tools used for studying turbulence is the simulation flow, known as isotropic turbulence. It is characterized by the absence of walls and has zero mean velocity. Moreover, we can model periodicity for all variables on all boundaries. One way to simulate isotropic turbulence is by adding a body force to the Navier-Stokes equations as follows:

$$\frac{\partial\,\bar{u}_i}{\partial\,t} = -\frac{\partial}{\partial\,x_j}\left(\bar{u}_i\bar{u}_j\right) - \frac{1}{\rho}\frac{\partial\,\bar{p}*}{\partial\,x_i} + \frac{\partial}{\partial\,x_j}\left[\nu_{ef}\left(\frac{\partial\,\bar{u}_i}{\partial x_j} + \frac{\partial \bar{u}_j}{\partial x_i}\right)\right] + \frac{\bar{f}_{bi}}{\rho}. \tag{35}$$

The procedure of forcing a flow is advantageous when working in Fourier space because it is possible to force only a band of wave numbers. This task is not trivial to perform in physical space, but in the Fourier space, it is possible impose this force to be zero outside the desired range of wave numbers (Eq. 38). The forcing method proposed by [Eswaran and Pope (1988)] was used. This choice was made in order to allow a spectral analysis of stationary turbulence. Therefore, it is possible to inject an amount of energy at the smallest wave numbers of the energy spectrum as follows [Eswaran and Pope (1988); Alvelius (1999); Smirnov, Shi, and Celik (2001)]:

$$\widehat{\bar{f}}_{bi}\left(\boldsymbol{k},t\right) = \wp_{ij}\left(\boldsymbol{k}\right) W_j\left(\boldsymbol{k},t\right) \theta\left(\boldsymbol{k}\right), \tag{36}$$

where $\wp_{ij}\left(\boldsymbol{k}\right)$ is the projection tensor defined in Eq. 21 and $\theta\left(\boldsymbol{k}\right)$ gives the limiting value for the forcing process to the wave numbers of interest, given by:

$$\theta\left(\boldsymbol{k}\right) = \begin{cases} 1 \quad \text{if} \quad k_{\text{inf}} \leq |\boldsymbol{k}| \leq k_{\text{sup}} \\ \\ 0 \quad \text{if} \quad |\boldsymbol{k}| \leq k_{\text{inf}} \text{ or } k_{\text{sup}} \leq |\boldsymbol{k}|, \end{cases} \tag{37}$$

where k_{inf} is the lower limit and k_{sup} is the upper limit of the wave number over which the force is imposed. It remains to define $W_j(\boldsymbol{k},t)$, which is the Uhlenbeck-Örnstein process of stochastic diffusion [Eswaran and Pope (1988)]. This process is characterized by a scale of temporal decorrelation (T_L) and a parameter that models the amplitude (σ) of the fluctuations.

The equation for the spectral density of turbulent kinetic energy $(E_k(\boldsymbol{k},t))$ for an isotropic turbulence flow is given by Eq. 38 [(Lesieur, Métais, and Comte, 2005)]:

$$\left(\frac{\partial}{\partial t}+2\nu k^2\right)E_k(\boldsymbol{k},t)=T(\boldsymbol{k},t)+f_{bk}(\boldsymbol{k}) \tag{38}$$

where $f_{bk}(\boldsymbol{k})$ is the energy injected by the forcing term $f_{bi}(\boldsymbol{k})$ (Eq. 36)) and $T(\boldsymbol{k},t)$ is the nonlinear transfer rate of turbulent kinetic energy between the turbulent structures of wave number $\boldsymbol{k}$ with all other structures of the spectrum. When the spectrum is not completely solved, this term is decomposed into the following:

$$T(\boldsymbol{k},t)=T_r(\boldsymbol{k},t)+T_{sg}(\boldsymbol{k},t), \tag{39}$$

where $T_r(\boldsymbol{k},t)$ is the nonlinear energy transfer between the resolved turbulent structures and $T_{sg}(\boldsymbol{k},t)$ is the energy transfer between the resolved and the sub-grid turbulent structures. This process is usually modeled by $T_{sg}(\mathbf{k},t)=-2\nu_t k^2 E_k(\mathbf{k},t)$. Assuming stationary turbulence,

$$\int_0^{k_c} T_r(\boldsymbol{k})\,d\boldsymbol{k}=0. \tag{40}$$

The energy injected into a spectrum band $(k_{inf}\leq k_i\leq k_{sup})$ yields the following balance:

$$\int_0^{k_c}\left(2\nu k^2\right)E_k(\boldsymbol{k})\,d\boldsymbol{k}+\int_{k_c}^{\infty}\left(2\nu_t k^2\right)E_k(\boldsymbol{k})\,d\boldsymbol{k}=\int_{k_{inf}}^{k_{sup}} f_{bk}(\boldsymbol{k})\,d\boldsymbol{k}. \tag{41}$$

Once energy is injected into the spectrum, it is nonlinearly transferred to smaller structures, up to the level of the dissipative scales. When it reaches steady state, the energy spectrum is sustained because the injection supplies, at the same rate, the nonlinear transfer and the dissipated energy of the spectrum (Eq. 41). The nonlinear mechanism of energy transfer promotes an important physical mechanism known as an energy cascade. The energy is transferred in a nonlinear way, up to the Kolmogorov dissipative scales, where it is dissipated by viscous effects. In the studies

of isotropic turbulent flows, the theory of [Kolmogorov (1941)] assumes the equilibrium hypothesis, where all the energy injected into the spectrum is dissipated by viscous effects. The balance can be achieved only for statistically stationary turbulent flows. Kolmogorov's theory establishes that the spectrum of turbulent kinetic energy in its inertial region takes the following form:

$$E_k(\boldsymbol{k}) = C_k \varepsilon^{2/3} \|\boldsymbol{k}\|^{-5/3}, \tag{42}$$

where $E_k(\boldsymbol{k})$ is the energy spectrum, ε is the rate of viscous dissipation, $C_k = 1.4$ is the Kolmogorov constant and $\|\boldsymbol{k}\|$ is the norm of the wave number vector. Thus, comparing the energy spectrum obtained numerically for a given turbulent flow with Kolmogorov's law is one of the most frequently utilized procedures for validating the turbulence modeling method; for instance, with models that use the *LES* methodology. This validation has the main goal of evaluating the energy spectrum in the inertial zone, under the regime of stationary turbulence. For this, the body force should be random and restricted to larger scales (low wave numbers). It does not interfere in the rest of the spectrum, which attempts to simulate the $k^{-5/3}$ Kolmogorov's law. In addition to this step, a qualitative verification is performed by comparing the vorticity modulus with the reference data of [Lesieur (1997)].

Table 1 shows the values used for the previously described parameters. These values were also chosen by [Sampaio (2006)] and used to validate a proposed turbulence model. In the present study, the same values were used because a detailed study of the influence of each parameter over the simulated flow is not a goal of the present work.

Table 1: Parameters used in the simulations of homogeneous and isotropic turbulence.

Parameters	Used value
$k_{\text{inf}}\left[m^{-1}\right]$	1
$k_{\text{sup}}\left[m^{-1}\right]$	3
$T_L[s]$	$0,1$
$\sigma\left[m/s^2\right]$	50
$\nu\left[m^2/s\right]$	10^{-6}

In all simulations, the calculation domain is given by $L_x = L_y = L_z = 2\pi$. Periodic boundary conditions were used in all coordinates directions. The time step (Δt) was calculated using a diffusion time step Δt_d (Eq. 43) and an advective Δt_{ad} (Eq. 44), and it was corrected by the CFL criterion that provides stability to the time advance

process [Courant, Friedrichs, and Lewy (1967)] (Eq. 45):

$$\Delta t_d = \frac{1}{2\nu}\left(\frac{1}{\Delta x^2}+\frac{1}{\Delta y^2}+\frac{1}{\Delta z^2}\right)^{-1}, \tag{43}$$

$$\Delta t_{ad} = \min\left[\frac{\Delta x}{\|u\|_{\max}}, \frac{\Delta y}{\|v\|_{\max}}, \frac{\Delta z}{\|w\|_{\max}}\right], \tag{44}$$

$$\Delta t = CFL \min\left[\Delta t_d, \Delta t_{ad}\right]. \tag{45}$$

The parameter CFL is a number between 0 and 1. For the simulations presented in the present work, $CFL = 0.95$ was used. Thus, starting from a velocity field of zero values, the body force (f_{bi}) was used to accelerate the flow, and large turbulent structures were formed inside the domain. These structures transfer energy for the entire spectrum of the turbulent structures, leading to the transfer of energy up to the Kolmogorov dissipative scales. Until it reaches the Kolmogorov length scales, practically no energy is dissipated. It is mainly transferred to structures of different sizes by the nonlinear mechanism. This is a physical process that can be simulated using the *DNS* methodology. When the *LES* methodology is used, the modeling of turbulence enables the transfer of energy through the cutting scales, determined by the used grid. This determines the so-called "grid filter" cutoff frequency or cutoff wave number. When the steady state is reached, in the statistical sense, the injected energy must be equal to the dissipated energy at a dissipation rate ε.

Alternately, the simulation starts from a velocity field generated by random disturbances, restricted to a small band of low wave numbers of the energy spectrum. This procedure can be used to reduce the processing time. The qualitative analysis of the flow in each studied case was performed through isosurface visualisations of the vorticity module. The quantitative analysis was performed over the turbulent kinetic energy spectra of the simulations at different times, calculated according to the methodology proposed by [Pope (2000)], from the velocity fields in Fourier space.

Figure 5 (a) shows the temporal evolution of the turbulent kinetic energy spectrum for a simulation without turbulence modeling. For the previously described velocity fields generated by random disturbances, an amount of energy is injected via a forcing term. Note that the energy accumulates over the higher wave numbers of the spectrum, up to the numerical divergence of the simulation. Note that without the use of sub-grid turbulence modeling, this behavior was expected. This is because the developed pseudo-spectral code is free of numerical diffusion. The numerical viscosity also models the energy transfer between the frequency or wave number bands. In the spectrum, a straight line with a $k^{-5/3}$ slope is also shown for reference. One observes the energy accumulation in the band of high wave numbers because

of the absence of adequate energy transfer. It can be seen for $t = 2[s]$ and $10[s]$ that the energy spectrum is physically inconsistent, showing very high energy levels at the higher wave numbers. The smallest structures of turbulence have more energy than the largest structures, i.e., smaller wave numbers. This is a consequence of the inadequate energy accumulation in the cutoff frequencies because of the absence of sub-grid scale modeling. Figure 5 (b) shows the vorticity modulus; the presence of numerical noise is noticed because the energy accumulates in the higher wave numbers.

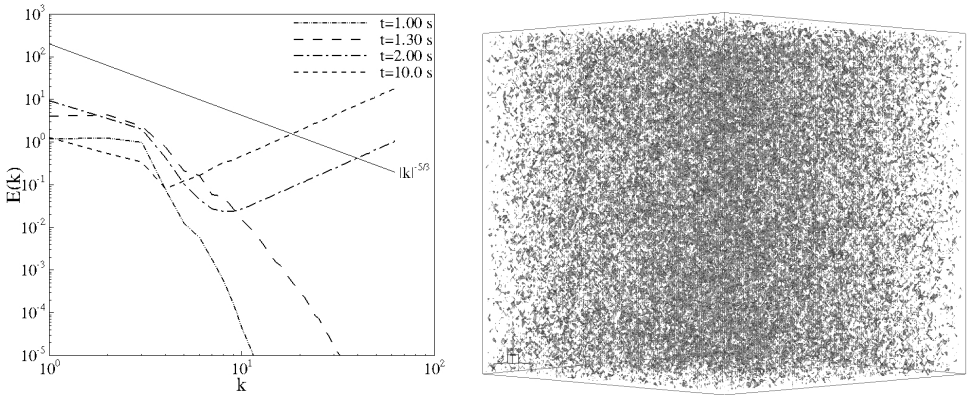

(a) (b)

Figure 5: Numerical simulation without sub-grid turbulence modeling: (a) temporal evolution of the turbulent kinetic energy spectrum and (b) the vorticity at $t = 10[s]$.

The absence of modeling results in physical inconsistency. Therefore, the goal now is to show that the correct use of turbulence modeling yields physically consistent results. Figure 6 shows the behavior of the methodology with three levels of refinement, changing the number of collocation points, i.e., 32^3, 64^3 and 128^3. Dynamic sub-grid scale modeling was used for all simulations, starting from the initial velocity fields. The flow is forced through a body force given by Eq. 36 and with the parameters given in Tab. 1. The simulations continue until a statistically established regime ($t = 6[s]$) is reached. Figures 6 (a), (b) and (c) show the vorticity module for the grids of 32^3, 64^3 and 128^3, respectively. Note that with 32^3 collocation points, the obtained eddy structures exhibit low-resolution topological traces. However, the energy spectrum is relatively well calculated, thanks to the combination of high accuracy and the sub-grid scale dynamic modeling used. As the number of collocation points is increased, smaller structures are captured, and the amount of captured structures increases considerably. The high level of detail for the captured physi-

cal structures with 128^3 collocation points is also noteworthy, compared with other simulations. Figure 6 (d) shows the spectra of turbulent kinetic energy for the three levels of refinement. The grid of 32^3 collocation points presents a small accumulation of energy in all of the spectra. This accumulation can be explained by the analysis of Eq. 41. Indeed, the smaller the cutoff wave number k_c the smaller the $\int_0^{k_c} \left(2\nu k^2\right) E_k(\boldsymbol{k})\, d\boldsymbol{k}$ term that must model the turbulent kinetic energy dissipated by viscous effects in the wave number band $(0 - k_c)$. Moreover, by decreasing k_c the contribution of the $\int_{k_c}^{\infty} \left(2\nu k^2\right) E_k(\boldsymbol{k})\, d\boldsymbol{k}$ term becomes bigger, which represents the dissipation of the turbulent kinetic energy by the "turbulent effects". This last term models, by the concept of turbulent viscosity, the nonlinear physical effects that are not calculated directly by the simulation. The smaller the k_c the smaller the number of solved structures and the greater the number of modeled structures. It is natural that the error promoted by sub-grid scale modeling increases as coarser grids are used. For 64^3 and 128^3 points, there was a decay in the energy level, and the spectra were closer. As the grid was refined, a greater proximity to the $k^{-5/3}$ Kolmogorov law was obtained. Because of this behavior for all subsequent simulations, the grid with 128^3 collocation points will be used.

Figures 7 illustrates the temporal evolution of the spectral density of turbulent kinetic energy obtained with dynamic Smagorinsky sub-grid scale modeling [Germano, Piomelli, and Moin (1991)]. Starting from a random velocity field, restricted to a range of wave numbers of the spectrum, an amount of energy is injected via a forcing term, which is transmitted to all wave numbers of the spectrum via a nonlinear process. The energy cascades until it reaches the cutoff scales of the grid filter. All simulations were performed until the flow reached a balance between injected and dissipated energy for a statistically stationary regime. The $\log\left(E_k(\boldsymbol{k})\right)$ and $\log(\boldsymbol{k})$ scales were used, and a straight line with a slope of $k^{-5/3}$ is also shown as a reference. One notes a good agreement with the Kolmogorov law for the times greater than $5[s]$ and that the flow remains steady after this time. This is typical of the balance between the injected energy, the transferred energy and the dissipated energy.

Figures 8 shows the isovalues of the vorticity modules for different times. Since the initial time, the flow presents turbulent structures, which, with the development of the simulation, are multiplied due to the nonlinear amplification process of disturbances, generating smaller and smaller structures. The flow reaches the turbulence state when the spectrum remains stationary and exhibits a $k^{-5/3}$ Kolmogorov law. At all times, coherent structures of turbulence can be observed. Figure 9 shows a qualitative comparison of the vorticity modulus between the present work and

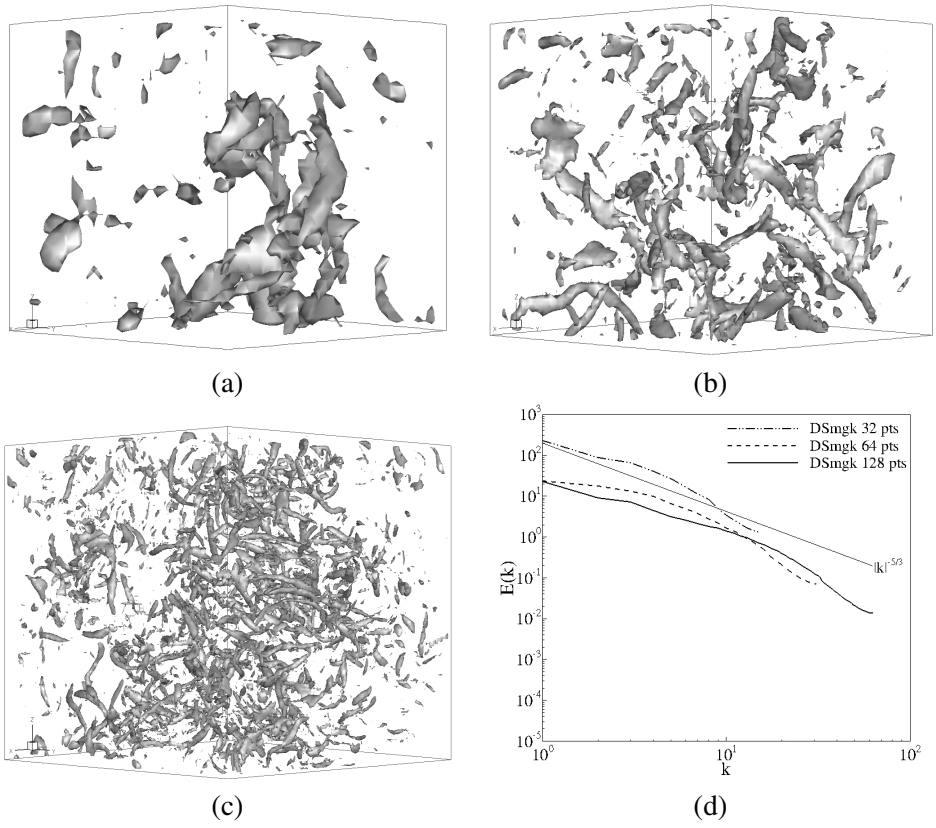

Figure 6: Influence of the collocation point number using the dynamic Smagorinsky sub-grid scale model; the vorticity module is visualized using (a) 32^3, (b) 64^3 and (c) 128^3 1283 collocation points; (d) spectral density of turbulent kinetic energy.

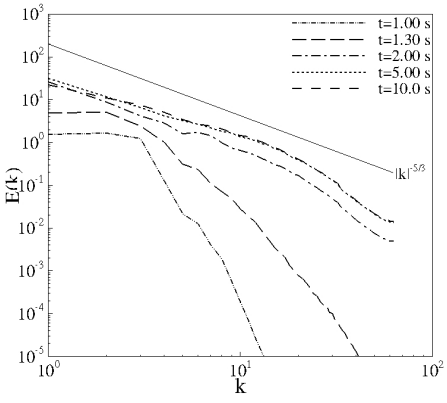

Figure 7: Temporal evolution of the turbulent kinetic energy spectrum using the Smagorinsky dynamic turbulence modeling.

that of Note the similarity between the structures in the form of filaments in both works; however, in the present work, there are a lot of smaller structures. This can be explained by the possible difference between the Reynolds numbers of the present study and the study of [Lesieur, Métais, and Comte (2005)], or even by the chosen surface of the vorticity modulus. This value was chosen in order to get the best visualization of the structures. This criterion was used in both works compared here.

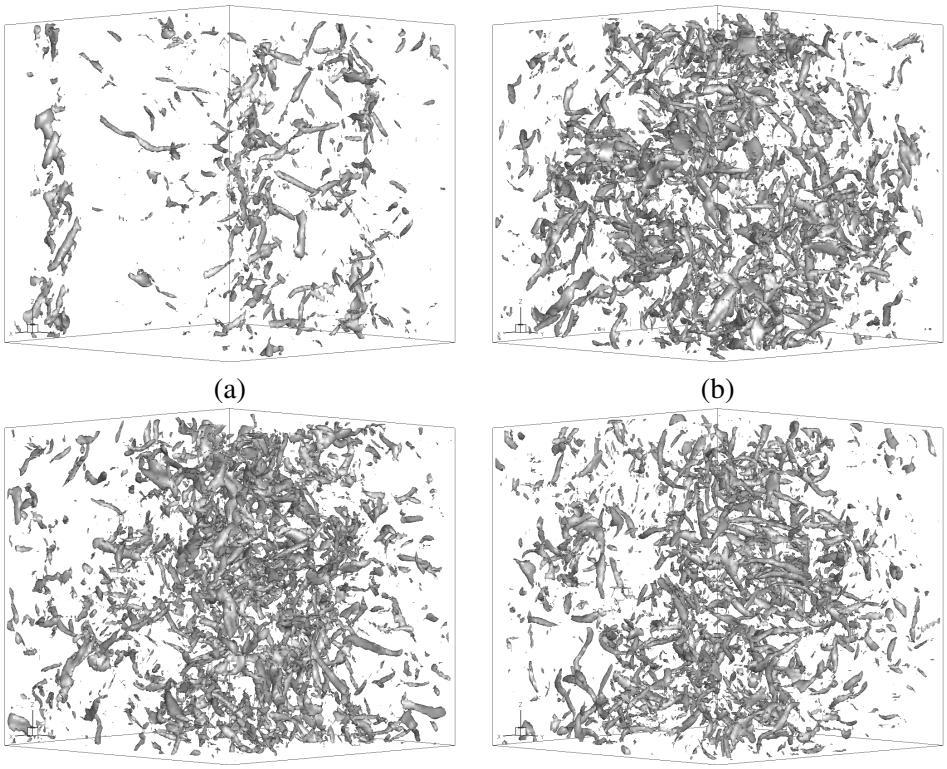

Figure 8: Temporal evolution of the vorticity modulus; simulation performed using the *LES* methodology with the dynamic Smagorinsky model: (a) t=2 [s], (b) t=4 [s], (c) t=6 [s] and (d) t=10 [s].

Figures 10 (a), (b) and (c) show the visualizations of the vorticity modulus at statistically stationary regimes, and Fig. 10(d) illustrates the spectra of turbulent kinetic energy. Sub-grid Smagorinsky modeling with three different values of C_s was used. These simulations were performed with the goal of adjusting the model constant. With $C_s = 0.10$, the modeling failed to transfer all of the energy required towards

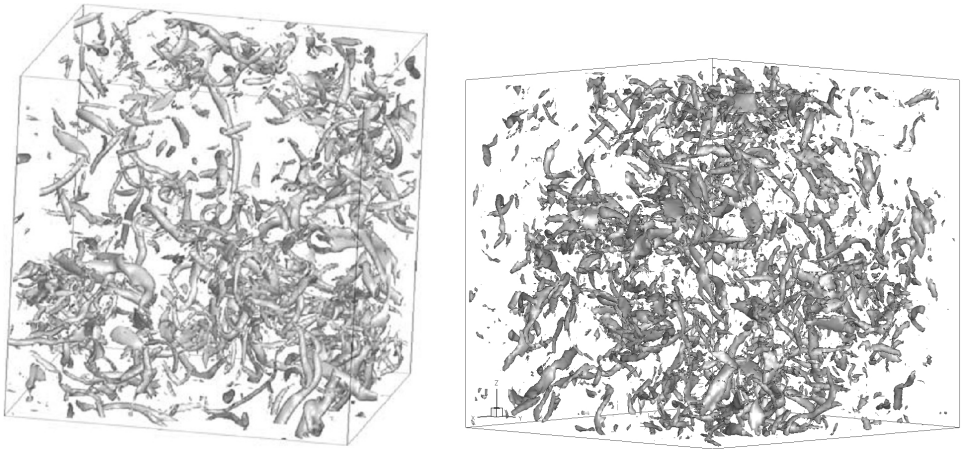

(a) (b)

Figure 9: Vorticity module for homogeneous and isotropic turbulence: (a) [Lesieur, Métais, and Comte (2005)] and (b) present work.

the sub-grid scales of turbulence, and an energy accumulation in the high frequencies of the spectrum was noted. The visualization of Fig. 10 (a) shows a large quantity of high-frequency turbulent structures, which does not correspond to the physical nature of the problem, as demonstrated by the energy spectrum. The simulation using $C_s = 0.30$ shows an excessive energy transfer, and the spectrum does not reach the slope of $k^{-5/3}$, except for a band very restricted to small wave numbers. In this case, Fig. 10 (c) shows that the energy was excessively dumped. The constant 0.18, calculated analytically by [Lilly (1992)], gives a good approximation to the Kolmogorov $k^{-5/3}$ law in a large part of the spectrum.

The purpose of these simulations and of the present paper is to show the importance of turbulence modeling and of the adjustment of the value of the Smagorinsky constant. A new value of this constant in a statistically stationary regime can be determined by dividing Eq. 10 by Eq. 12 and taking the spatial mean ($\langle\ \rangle$) of $C_{sd}(\boldsymbol{x},t)$, giving:

$$C_s(t) = \sqrt{\langle C_{sd}(\boldsymbol{x},t)\rangle}. \tag{46}$$

Using Eq. 46 and the simulations with the Smagorinsky dynamic model, the value $C_s = 0.12$ was determined for several different times. Therefore, this constant is indeed independent of time.

Figures 11 (a) and (b) show the vorticity modulus in the statistically stationary regime using Smagorinsky modeling with $C_s = 0.12$ and the dynamic Smagorinsky

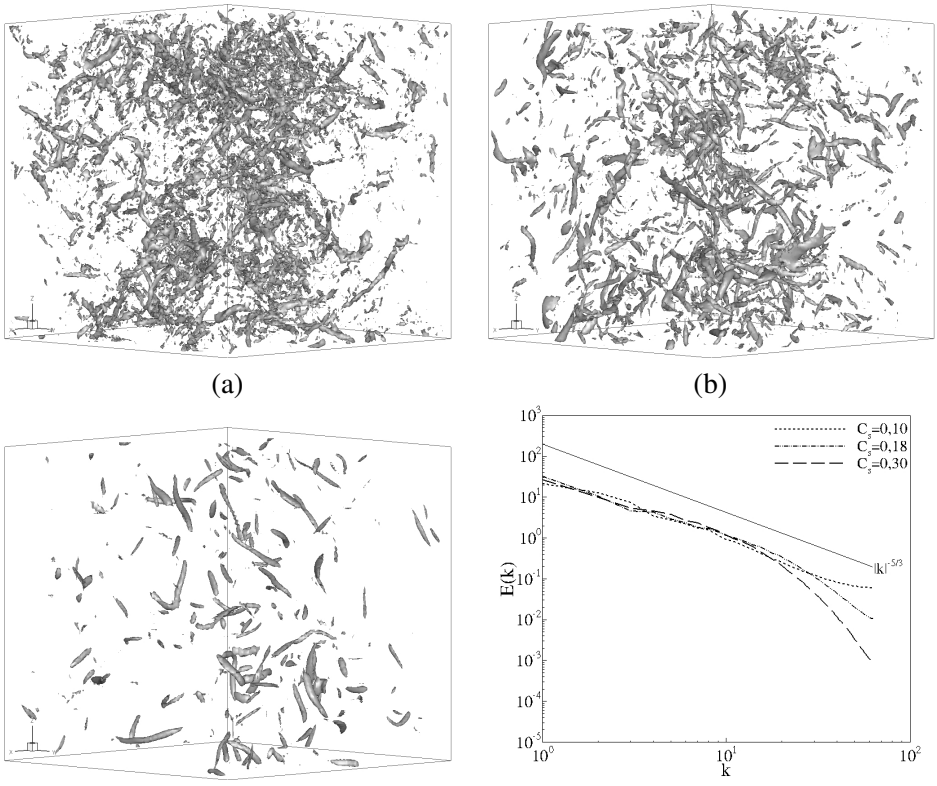

Figure 10: Influence of the Smagorinsky constant; vorticity module in regime statistically established: (a) $C_s = 0.1$; (b) $C_s = 0.18$ and (c) $C_s = 0.3$ and (d) spectra of turbulent kinetics.

model. Note a greater number of structures using Smagorinsky modeling. The turbulent structures obtained with Smagorinsky modeling are apparently noisier than those obtained with dynamic modeling, which are more coherent. A large quantity of characteristic structures of turbulence can be noted.

Figures 11 (c) and (d) present the turbulent kinetic energy spectra that were obtained using the Smagorinsky and dynamic Smagorinsky models. The spectrum obtained with Smagorinsky modeling approached the Kolmogorov law very well, but because of the numerical instabilities found in Fig. 11 (a), the dynamic model is still the best option. The adjustment of the constant proposed above serves as a way to optimize the use of the Smagorinsky model for a given numerical code based on the pseudo-spectral method.

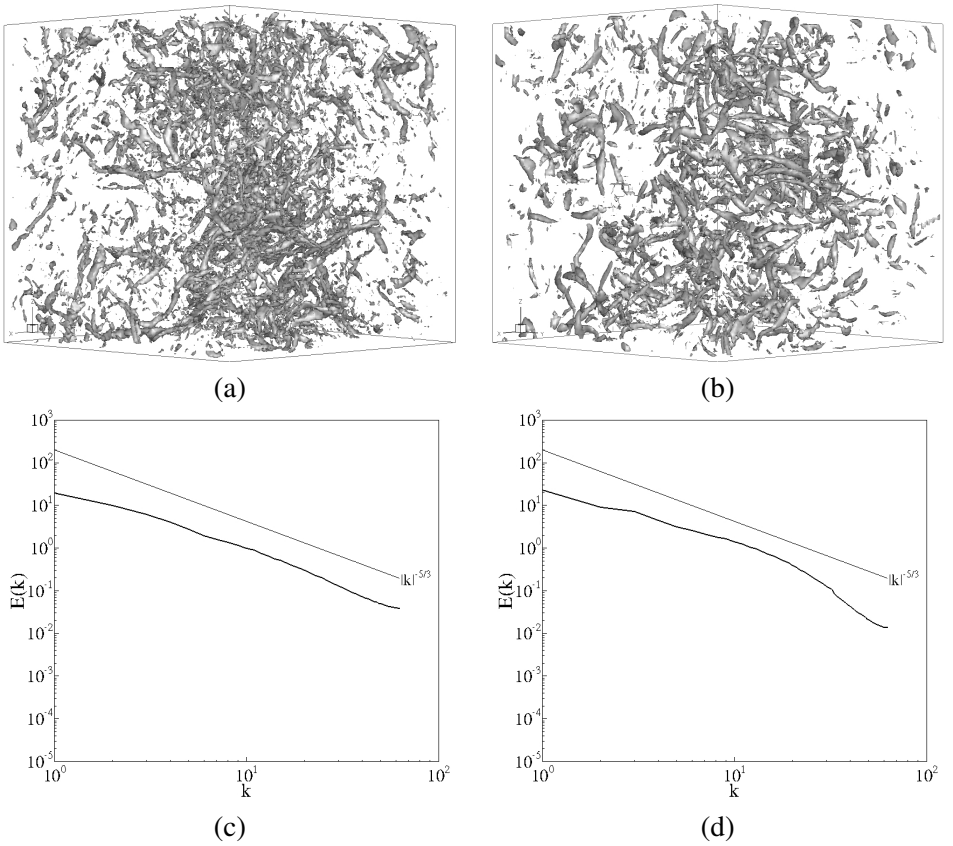

Figure 11: Comparison between the Smagorinsky model using $C_s = 0.12$ and the dynamic Smagorinsky model; the vorticity module is shown: (a) Smagorinsky model; (b) dynamic Smagorinsky model; (c) turbulent kinetic energy spectrum for the Smagorinsky model and (d) turbulent kinetic energy spectrum for the dynamic Smagorinsky model.

4 Conclusions

In the present study, the goal was to show the importance of correctly modeling turbulent flow. To do this, the isotropic turbulence in a box with periodic boundary conditions was simulated using the classic sub-grid Smagorinsky and the dynamic Smagorinsky modeling approaches. The temporal evolution of the turbulent kinetic energy spectra and the vorticity module were shown with and without turbulence modeling. When using the Smagorinsky model, one has to adjust its constant so that the energy transfer occurs correctly, compared with the Kolmogorov cascade

law. A way to determine the Smagorinsky constant was also proposed from the results obtained from simulations using the dynamic Smagorinsky model. Finally, a case in which no turbulence modeling is used was presented. In this case, the turbulent kinetic energy spectrum was completely inconsistent from a physical point of view. This illustrates once again the need for turbulence modeling when the spectrum is not completely solved. This is a consequence of the Fourier pseudo-spectral method that does not present numerical viscosity. Another way to achieve numerical stability would be to solve for the entire energy spectrum using the appropriate refinement in the discretisation process, i.e., to use direct numerical simulation.

Acknowledgement: The authors thank the College of Mechanical Engineering (FEMEC) of the Federal University of Uberlândia (UFU), CAPES, FAPEMIG, CNPq and PETROBRAS for financial support.

References

Allampalli, V.; Hixon, R.; Nallasamy, M.; Sawyer, S. D. (2009): High-accuracy large-step explicit Runge-Kutta (HALE-RK) schemes for computational aeroacoustics. *Journal of Computational Physics*, vol. 228, no. 10, pp. 3837–3850.

Alvelius, K. (1999): Random forcing of three-dimensional homogeneous turbulence. *Physics of Fluids*, vol. 11, no. 7, pp. 1880–1890.

Briggs, W. L.; Henson, V. E. (1995): *The DFT: an owner's manual for the discrete Fourier transform*. SIAM: Society for Industrial and Applied Mathematics.

Canuto, V. M.; Cheng, Y. (1997): Determination of the Smagorinsky-Lilly constant Cs. *Physics of Fluids*, vol. 9, no. 5, pp. 1368.

Ceniceros, H. D.; Roma, A. M.; Silveira-Neto, A.; Villar, M. (2010): A Robust, Fully Adaptive Hybrid Level-Set/Front-Tracking Method for Two-Phase Flows with an Accurate Surface Tension Computation. *Communications in Computational Physics*, vol. 8, no. 1, pp. 51–94.

Chen, C.; Chang, S.; Sun, S. (2007): Lattice boltzmann method simulation of channel flow with square pillars inside by the field synergy principle. *CMES: Computer Modeling in Engineering and Sciences*, vol. 22, pp. 203–215.

Cooley, J. W.; Tukey, J. W. (1965): An Algorithm for the Machine Calculation of Complex Fourier Series. *Mathematics of Computation*, vol. 19, no. 90, pp. 297–301.

Courant, R.; Friedrichs, K.; Lewy, H. (1967): On the Partial Difference Equations of Mathematical Physics. *IBM Journal of Research and Development*, vol. 11, no. 2, pp. 215–234.

da Silva, C. B.; Pereira, J. C. F. (2005): On the local equilibrium of the subgrid scales: The velocity and scalar fields. *Physics of Fluids*, vol. 17, no. 10, pp. 108103.

Eswaran, V.; Pope, S. B. (1988): An examination of forcing in direct numerical simulations of turbulence. *Computers & Fluids*, vol. 16, no. 3, pp. 257–278.

Germano, M.; Piomelli, U.; Moin, P. (1991): A dynamic subgrid scale eddy viscosity model. *Physics of Fluids A: Fluid Dynamics*, vol. 3, no. 7, pp. 1760–1765.

Henshaw, W. (1994): A fourth-order accurate method for the incompressible Navier-Stokes equations on overlapping grids. *Journal of computational physics*, vol. 113, no. 1, pp. 13–25.

Kolmogorov, A. N. (1941): The local structure of turbulence in incompressible viscous fluid for very large Reynolds number. *Doklady Akademii Nauk Sssr*, vol. 30, no. 4, pp. 301–305.

Lesieur, M. (1997): *Turbulence in Fluids*. Kluwer Academic Publishers, 3 edition.

Lesieur, M.; Métais, O.; Comte, P. (2005): *Large-Eddy Simulations of Turbulence*. Cambridge University Press, New York.

Lilly, D. (1992): A proposed modification of the Germano closure method. *Physics of Fluids A: Fluid Dynamics*, vol. 4, no. 3, pp. 633–635.

Maier, a.; Iapichino, L.; Schmidt, W.; Niemeyer, J. C. (2009): Adaptively Refined Large Eddy Simulations of a Galaxy Cluster: Turbulence Modeling and the Physics of the Intracluster Medium. *The Astrophysical Journal*, vol. 707, no. 1, pp. 40–54.

Mariano, F. P.; Moreira, L. d. Q.; da Silveira-Neto, A.; da Silva, C. B.; Pereira, C. F. (2010): A new incompressible Navier-Stokes solver combining Fourier pseudo-spectral and immersed boundary methods. *CMES: Computer Modeling in Engineering and Sciences*, vol. 59, no. 2, pp. 181–216.

Moreira, L. d. Q. (2007): *Simulação de Grandes Escalas de Jatos Periódicos Temporais Utilizando a Metodologia Pseudo-Espectral de Fourier*. Dissertação de mestrado, Universidade Federal de Uberlândia, 2007.

Parrish, I. J.; Quataert, E.; Sharma, P. (2010): Turbulence in Galaxy Cluster Cores: a Key To Cluster Bimodality? *The Astrophysical Journal*, vol. 712, no. 2, pp. L194–L198.

Pope, S. B. (2000): *Turbulent Flows*. Cambridge University Press, New York.

Sampaio, L. E. B. (2006): *Simulação de Grandes Escalas da Bolha de Separação em Placas Finas À Pequeno Ângulo de Incidência*. Doutorado em engenharia mecânica, Pontifícia Universidade Católica do Rio de Janeiro, 2006.

Silva, A. R.; Silveira-Neto, A.; Francis, R.; Rade, D. A.; Santos, E. A. (2009): Numerical Simulations of Flows over a Pair of Cylinders at Different Arrangements using the Immersed Boundary Method. *CMES: Computer Modeling in Engineering and Sciences*, vol. 50, no. 3, pp. 285–303.

Silva, H.; Souza, L.; Medeiros, M. (2007): Verification of a mixed high-order accurate DNS code for laminar turbulent transition by the method of manufactured solutions. *International Journal for Numerical Methods in Fluids*, pp. 1–6.

Smagorinsky, J. (1963): General circulation experiments with the primitive equations. *Monthly weather review*, vol. 91, no. 3, pp. 99–164.

Smirnov, A.; Shi, S.; Celik, I. (2001): Random flow generation technique for large eddy simulations and particle-dynamics modeling. *Journal of Fluids Engineering*, vol. 123, pp. 359.

Takahashi, D. (2006): A Hybrid MPI / OpenMP Implementation of a Parallel 3-D FFT on SMP Clusters. pp. 970–977.

Vedovoto, J. a. M. (2007): *Modelagem Matemática e Simulação Numérica de Escoamentos Incompressíveis sobre Geometrias Complexas Tridimensionais Utilizando o Método da Fronteira Imersa*. Master thesis, Universidade Federal de Uberlândia, 2007.

Villar, M. M. (2007): *Análise Numerica Detalhada de Escoamentos Multifásicos Bidimensionais*. Tese de douturado, Universidade Federal de Uberlândia, 2007.

White, F. M. (1991): *Viscous Fluid Flow*. McGraw-Hill, New York United States of America, 2 edition.